CRUSTAL EFFECTS ON REGIONAL SEISMIC PHASES IN ASEISMIC REGIONS OF NORTHERN EURASIA: CONSTRAINTS FROM PNE RECORDINGS

Igor B. Morozov, Scott B. Smithson, and Elena A. Morozova

Department of Geology and Geophysics, University of Wyoming, PO Box 3006, Laramie, WY, 82071-3006

Sponsored by U.S. Department of Defense
Defense Threat Reduction Agency

Grant No. DSWA01-98-0015

ABSTRACT

The University of Wyoming database of seismic recordings of Peaceful Nuclear Explosions (PNEs) has been recently extended to 19 PNEs recorded along 7 long-range refraction/reflection profiles: QUARTZ, CRATON, KIMBERLITE, RIFT, METEORITE, and RUBY (2 lines). These profiles form a grid traversing the East European Platform, the Ural Mountains, the West Siberian Basin, the Baikal Rift, and the Siberian craton in two directions,., and include dense and reversed linear as well as fan PNE recordings (RUBY). Dense, 3-component recordings along subparallel and crossing profiles provide us with unique opportunities to study large-scale propagation effects of regional seismic phases, allow detailed examination of the regional seismic phases, correlation between the individual PNE records and with geologic and tectonic features.

In this report, we extend traditional, travel-time analysis of PNE arrivals to amplitude and waveform inversion and show how short-period PNE recordings are used to constrain the effects of crustal structure on seismic arrivals within 1000 - 3000 km ranges. These new constraints include (1) characterization of crustal attenuation through coda measurements and (2) imaging of the crustal structure using receiver function techniques. Both of these factors are of primary importance for modeling of crustal-guided phases, such as the P_g and L_g,

Energy-balance considerations in three dimensions show that an extensive coda is inherent to all *P*-wave phases. This coda can be explained by crustal scattering and is a result of effectively areal excitation of short-period scattered waves (P_g, S_g, L_g, R_g) within the crust by the waves incident from the mantle, or, conversely, by generation of mantle phases from crustal-guided waves within a distributed source region. The resulting estimates of coda Q range between Q=380 near 2 Hz and Q=430 around 5 Hz and can be associated with crustal attenuation. Our coda model also explains the observed build-up of the arrival amplitude with time and the apparent lack of a pronounced coda of body-wave arrivals from the mantle transition zone. We "deconvolve" the overlapping codas of the arrivals and extract their true relative amplitudes. These coda-free amplitudes could potentially be used in improved seismic discriminants.

In order to constrain the principal crustal structures from regional and teleseismic PNE arrivals, we show that scattering and P/S conversions within the crust cause reverberations in the waveforms of *P*-wave arrivals. Stacking of receiver functions of first arrivals results in consistent images of the basement along the PNE profiles. In another consequence, variation of the sediment/basement contact is a major factor influencing the complexity of PNE arrivals that may influence both amplitude and frequency characteristics of seismic discriminants.

This study demonstrates that amplitudes and waveforms of PNE records provide valuable quantitative constraints on crustal structure for the analysis of the propagation of L_g and other phases and for development and calibration of regional seismic discriminants.

Key Words: Peaceful Nuclear Explosions, Russian Eurasia, Crust, Scattering, Attenuation, Receiver Functions

OBJECTIVE

During the past several years, supported by the grants from the Air Force Office for Scientific Research (F49620-94-1-0134 and F49620-94-A-0134) and from the Defense Threat Reduction Agency (DSWA01-98-0015) the University of Wyoming has acquired an impressive data set of seismic recordings of Peaceful Nuclear Explosion along a grid of linear profiles in Northern Eurasia (Figure 1). These unique seismic data are being investigated for their potential use in CTBT monitoring.

Until recently, apart from observations of *Lg* and *S* waves and their amplitude measurements (Morozov et al., 1997, 1999), PNE records were analyzed primarily as wide-angle seismic data, with an emphasis on travel-time modeling and inversion. In this report, we focus our attention on the amplitude and waveform pattern of the PNE wavefield and investigate applicability and usefulness of coda amplitude measurements and receiver function techniques traditionally employed in teleseismic studies. Our objective in the following is to demonstrate that (1) these methods allow constraining variations of the depth of the basement and crustal attenuation – crustal features that are critical for *Lg* modeling and seismic path calibration, and (2) accounting for coda effects allows obtaining coda-free amplitudes of secondary phases (P_g, *PP*, *S*, L_g) that could be used in improved seismic discriminants.

RESEARCH ACCOMPLISHED

Of the seven PNE lines in Figure 1, QUARTZ has been studied the best, with detailed crustal and upper

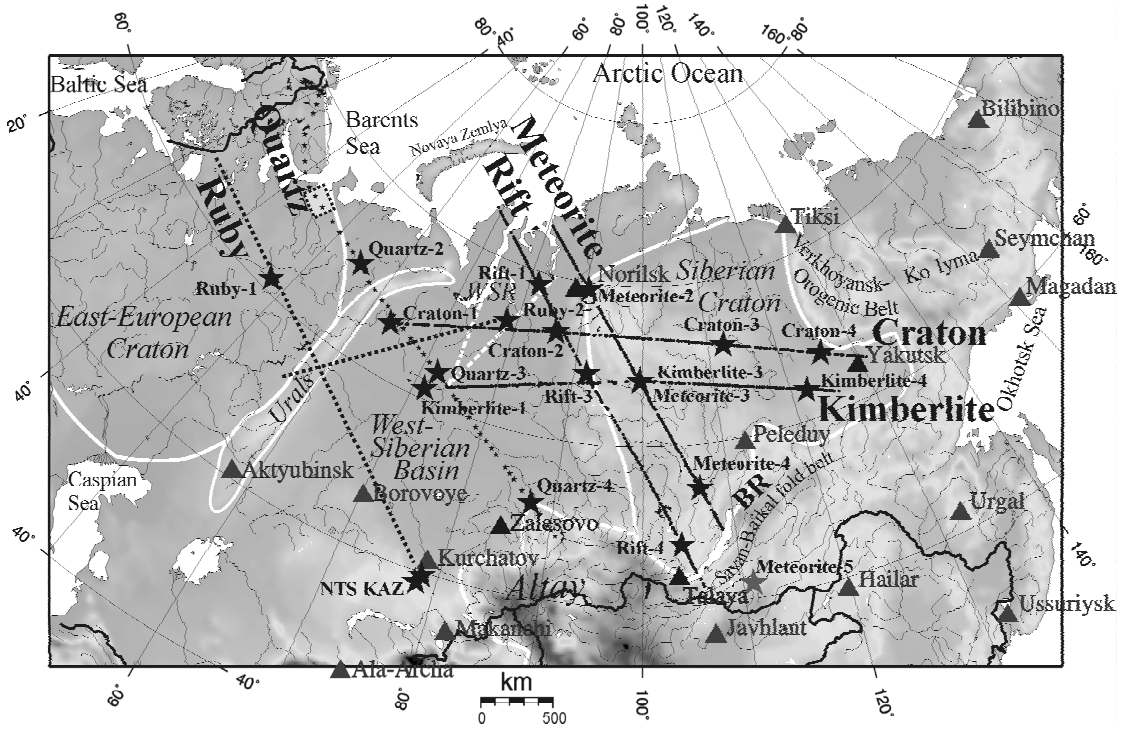

Figure 1 DSS PNE profiles under study at the University of Wyoming: QUARTZ, CRATON, KIMBERLITE, RIFT, METERORITE, and RUBY (two lines, obtained recently). Large stars are the PNEs, small stars (for profile QUARTZ only) are the chemical explosions. Profile RUBY is shown schematically. The coordinates and other parameters of the PNEs used in these profiles were reported by Sultanov et al. (1999). Major tectonic units are indicated in white contours (WSR – West Siberian Rift, BR – Baikal Rift).. Note the extent of systematic, continuous profiling, with PNEs detonated at the nodes of a 2-D recording grid. Also note that the profiles are close to some of the IMS stations (labeled triangles). The study of crustal effects presented here was performed for profile QUARTZ. The box NW of PNE QUARTZ 2 indicates the area where crustal attenuation was measured using coda amplitude analysis.

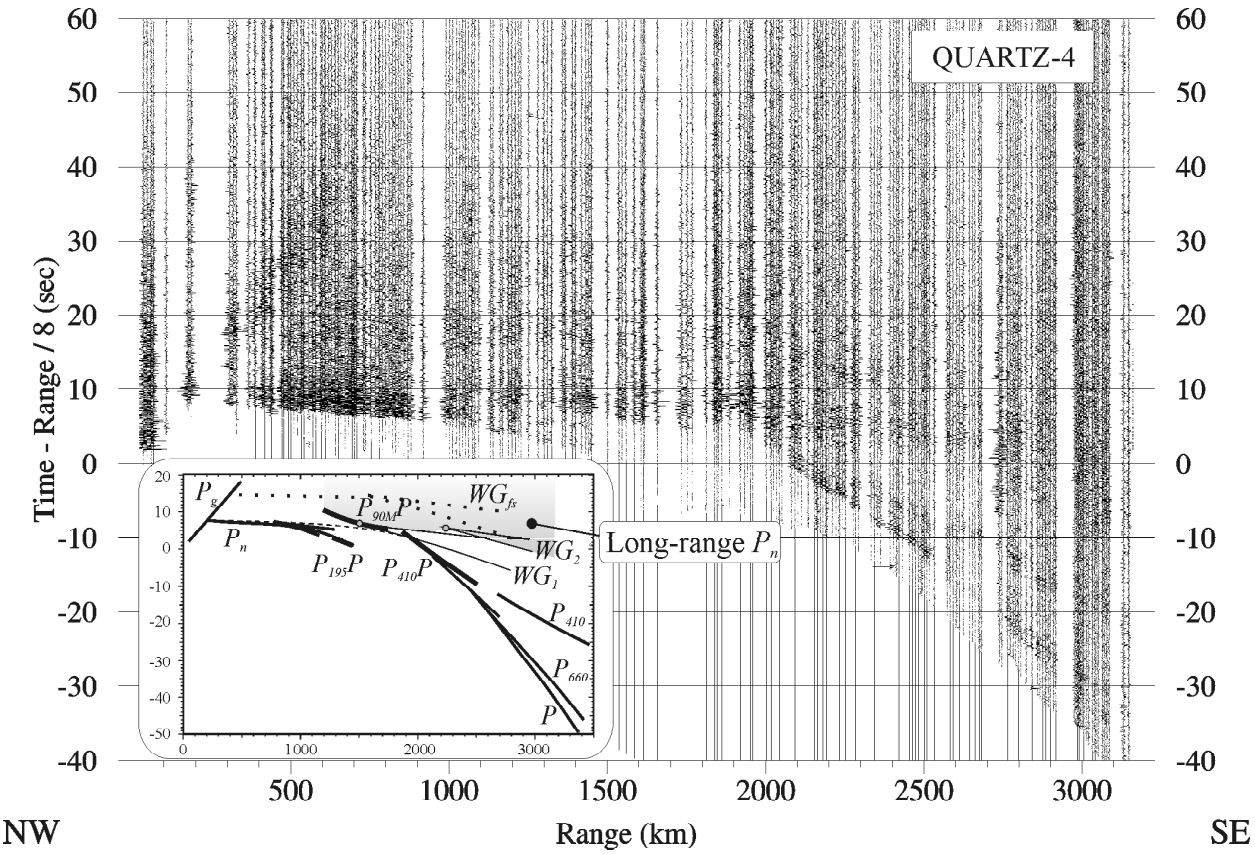

Figure 2 Vertical-component record from PNE QUARTZ-4 (Figure 1). Inset shows a sketch of typical refracted, reflected arrivals and their multiples identified in the PNE wave pattern. Note the strong second phases in the record. The long-range P_n phase (shaded in the inset) consists of arrivals forming a strong band of energy propagating to 3000 km at a group velocity between 8.0 – 8.1 km/s, with a faster branch at 8.5 km/s beyond 2700 km (Morozov *et al.*, 1998a). Note the unusually high energy of the arrivals in the primary P_n branch supporting the interpretation of the long-range P_n as a series of Moho and free-surface multiples of P_n and P_N (labeled *WG* and WG_{fs}). Also note that the long-range P_n phase is strong and is followed by a coda extending beyond the ends of records shown here.

mantle models developed, and this profile will be used in the following analysis. For our interpretation of the amplitude character of a "typical" PNE wavefield (Figure 2), we extract amplitude decay curves from several seismic records from PNE QUARTZ-4 (often also referred to as PNE 323) and CRATON (Figure 1 and Figure 3), between the offsets of 2000 – 2500 km. At these offsets, the separation of the phases provides the best illustration of the PNE energy pattern (Figure 2). The energy in the PNE wavefield at this distance appears to build up for 20 – 30 s after the first arrivals, followed by an extensive coda that can be observed for 100 – 150 s (Figure 3). Both the high amplitudes of the WG phases and the coda are surprising and must be understood in the context of future amplitude modeling of PNE records. Specifically, we will need to explain two features of the recorded distribution of PNE energy in Figure 3:

1) The long-duration codas of the observed codas of PNE arrivals. The coda of the free-surface multiple *PP* (WG_{fs} in our notation) appears much stronger than the coda of $P_{410}P$ reflections of nearly the same amplitude.

2) The apparent excess in the amplitudes of the WG phases compared to the reflections from the transition zone. Recent 1-D modeling (Mechie *et al.*, 1993; Morozova *et al.*, 1999).showed much lower amplitudes.

1. Coda decay rate of the PNE arrivals

A simple physical model of the coda allows us to obtain meaningful estimates of crustal attenuation quality factor (Q) and of the relative amplitudes of the arrivals without presently impractical 3-D finite-difference modeling. Our approach follows coda models accepted in teleseismic array observations (e.g., Greenfield, 1971; Bannister et al., 1990; Dainty, 1990; Gupta et al., 1991) and is based on two main observations. Firstly, waves propagating through the mantle and incident on the crust at high apparent velocity form a source of scattered energy different from the point-source model commonly used in coda estimates. Thus a correct coda model must take into account the distributed character of its excitation. Secondly, despite their apparent difference, we postulate that *all* the mantle arrivals could have similar coda patterns. Due to their long extent, these codas overlap contributing to the stepwise increase in energy seen in Figure 3. Decomposition of the recorded amplitude pattern allows us to obtain the true relation between the amplitudes of the onsets of the different PNE phases and their codas.

Figure 3 shows that the two *WG* multiples forming the long-range P_n are clearly distinct in the character of their codas. The first, Moho multiple labeled *WG* in Figure 2 is followed by a coda that dominates the record after high-pass filtering. However, in the low-frequency band, the strongest phase is the free-surface P_n multiple (WG_{fs}) followed by its coda. The higher amplitude of the WG_{fs} event is consistent with higher reflectivity of the free surface compared to the Moho. Also, the longer and low-frequency coda of WG_{fs} suggests a predominance of surface waves that propagate efficiently at lower frequencies and are progressively more attenuated as the frequency increases; this observation thus points to predominantly crustal origin of the coda.

Previous measurements of coda decay rate (Ryberg *et al*., 1995; Ryberg and Wenzel 1999) resulted in very high Q values over 1000 - 2000. However, we suggest that these values of Q might be overestimated from the use of a coda power decay rate (Aki and Chouet, 1975):

$$P(t) \propto t^{-\zeta} e^{-\omega t / Q}, \qquad (1)$$

where t is the time after the arrival, ω is the frequency. In expression (1), the factor $t^{-\zeta}$ with $\zeta \geq 1$ describes the geometric spreading of the waves forming the coda, and the quality factor Q corresponds to the attenuation. Ryberg and Wenzel (1999) used a preset value of $\zeta = 2$ assuming body-wave nature of the coda waves and a point source. However, as pointed out by Morozov *et al*. (1998a), the energy of the coda of the long-range PNE phases is better described by a relation (1) with $\zeta \approx 1.0$ for the higher-frequency coda and $\zeta \approx 0.9$ for the lower-frequency coda, with $Q=\infty$. This ambiguity in the determination of the attenuation factor Q using equation (1) illustrates the importance of a correct model of geometrical spreading. The tendency of the geometric spreading parameter ζ to values lower than 1 when $Q=\infty$ shows that formula (1) may not be applicable to the coda decay rate of the long-range PNE arrivals.

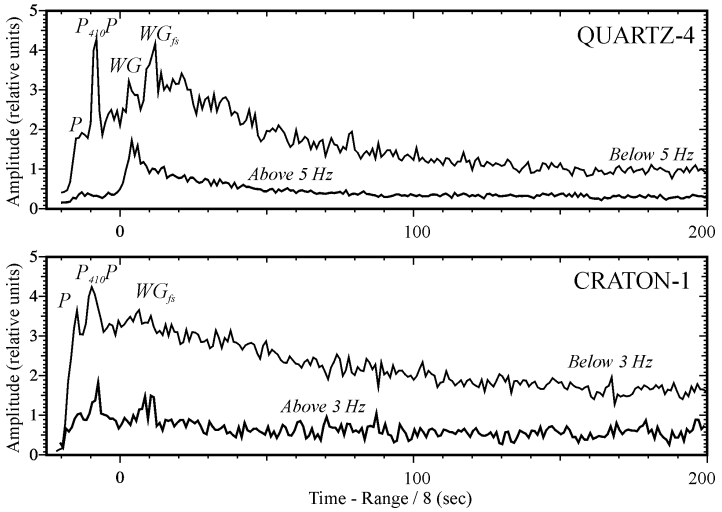

Figure 3 Amplitude of the high-frequency and low-frequency (filter corner frequency is 5 Hz for QUARTZ and 3HZ for CRATON) records within the offset range 2500 - 2600 km from PNE QUARTZ-4 and CRATON-1 (modified from Morozov and Smithson, in press). Time reduction is 8 km/s, and 7 three-component instantaneous trace amplitude records were averaged within a 2-s sliding time window and within the offset range (Morozov and Smithson, 1996) was used. First arrivals, a reflection from the 410-km discontinuity, and two whispering-gallery phases (*WG* and WG_{fs}) are indicated. Note the difference of the codas following the free-surface multiple refraction WG_{fs} at low frequencies and the Moho multiple *WG* at high frequencies. Note the about 150-sec long codas following the arrivals; also note the differences in these codas between the high- and low-pass filtered records and also between the PNEs.

Assuming predominantly crustal origin of the coda waves, coda amplitudes of PNE arrivals in Figure 2 can be explained readily once we take into account that seismic waves propagating through the mantle and entering the crust form a source of scattered waves that is different from a point source implied by relation (1). High apparent velocity of the incident waves (8 – 10 km/s) exceeds the velocity of the crustal-guided waves (3.5 – 5.5 km/s) generated through conversions on the Moho, on the basement, on surface topography, and on other velocity heterogeneities. Note that the most efficiently propagating phases within the crust (in the frequency range 0.5 - 10 Hz), post-critically reflected *S* waves, or L_g (Campillo, 1987), tend to the lower limit of this velocity range.

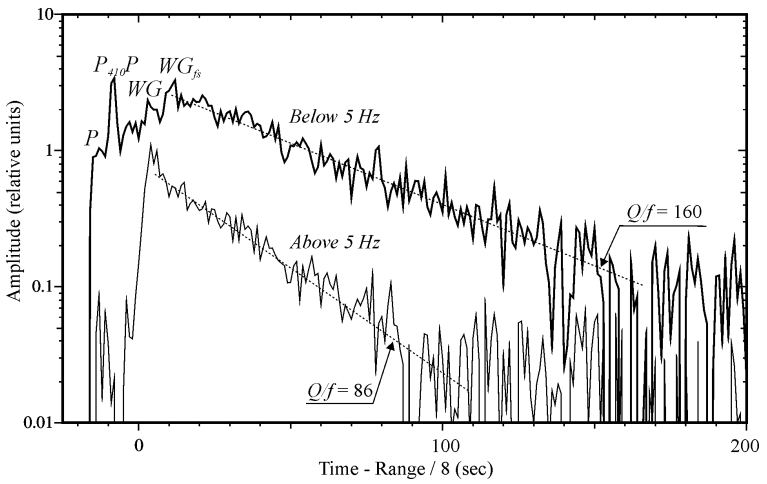

Figure 4 The same amplitudes as in Figure 3 plotted in logarithmic scale. Straight lines correspond to the relation (2) with $Q \approx 320$ for the low-frequency curve (at approximately 2 Hz) and $Q \approx 430$ for high frequency (at 5 Hz). Background noise estimated from a time window between 300- 350 s of the records was subtracted from both records prior to taking logarithm.

Since the apparent velocities of the incident mantle waves are much higher than the velocity of crustal-guided phases, we can approximate the generation of scattered energy within the crust and on the Moho as nearly simultaneous. The area of this distributed source of scattered energy increases with time, and thus the geometric spreading in coda decay cancels out and the entire decay of coda amplitude is due to the crustal attenuation:

$$P(t) \propto \tilde{P}(t) = e^{-\omega t/Q}. \qquad (2)$$

For more detail on the derivation of this coda power decay relation, see Morozov and Smithson (in press); a similar relation for coda energy was also obtained by Dainty (1985).

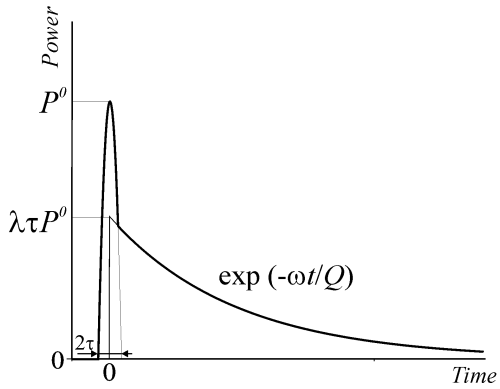

Figure 5 A model of intensity variation with time for a PNE event (see equations (3)). The energy of the primary event is approximated by a parabolic function and is characterized by its peak power P^0 and duration τ. The coda is parameterized by its coupling to the primary event λ and by its decay rate ω/Q defined in relation (2).

Relation (2) shows that the coda power decay law is purely exponential, in good agreement with the data throughout the entire observed duration of the coda. These linear trends of $\ln P(t)$ are consistent with log-RMS coda shapes of Semipalatinsk nuclear explosions presented by Baumgardt (1985). From this relation frequency-dependent *Q* can be easily estimated (Figure 4), resulting in values ranging from Q=320 near 2 Hz and Q=430 around 5 Hz. These values above suggest a dependence of $Q \approx 270 \cdot f^{0.3}$. and further confirm our association of the arrival PNE coda effects with crustal, preferably $P \rightarrow L_g$ or $L_g \rightarrow P$ scattering (Singh and Herrmann, 1983; Dainty, 1990). The comparatively low values of *Q* might be related to the effect of the thick sedimentary cover of the Pechora basin sampled by the part of the profile used in this analysis (Morozova *et al*., 1999).

2. True amplitudes of PNE phases

Since second arrivals ride on top of the codas of the earlier phases, the PNE record section exhibits a characteristic energy buildup, with the onsets of later phases appearing stronger than they are in reality. For the use

of these amplitudes in seismic discriminants, more stable estimates would apparently arise from the amplitudes that are free from such crustal contributions. As we show below, such "coda-free" amplitudes can be obtained by "deconvolving" the observed averaged amplitude.

In a simplified approach to such deconvolution, we again start from the localized amplitude decay curves shown in Figure 3, and model each of the events as a superposition of a primary arrival and of its coda (Figure 5). We assume that coda power follows the time dependence (2) and is proportional to the total energy of the primary phase. This approximation leads to a two-parameter amplitude decay model for each of the four arrivals labeled in Figure 3:

$$P(t-t^0)=\begin{cases} 0, & t<t^0, \\ \lambda P^0 \tau \tilde{P}(t-t^0), & t \geq t^0, \end{cases} \qquad (3)$$

where t^0 is the onset time, P^0 is the squared amplitude of the onset, τ is the estimated duration of the primary phase (so that $P^0\tau$ measures its total energy), and λ is the relative coda amplitude parameter. Since we assume that the mechanism of scattering is common for all arrivals, λ is the same for P, $P_{410}P$, WG, and WG_{fs}.

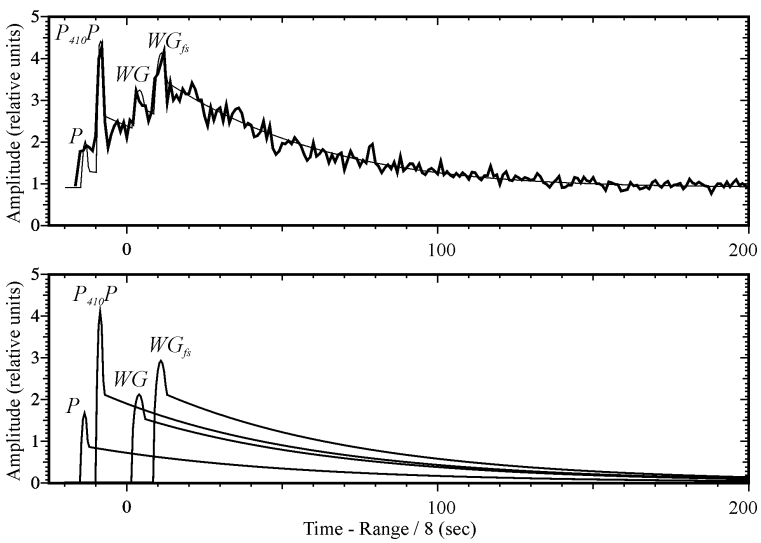

Figure 6 *Top*: Coda amplitude decay model for frequencies below 5 Hz. Thick line is the low-frequency amplitude from Figure 3, thin line shows the modelled amplitude shown in Figure 6. Note that crustal scattering and a simple approximation of coda power (1) explain the observed coda build-up by the subsequent *P*, $P_{410}P$, *WG*, and WG_{fs} arrivals. *Bottom*: Amplitudes and codas of the four separate arrivals forming the total coda energy. Note that this decomposed section is dominated by the reflection $P_{410}P$. Also compare the amplitude of *WG* in this plot to the high-frequency WG coda in Figure 3 and note that *WG* is stronger at lower frequencies, as expected.

By varying the parameters describing the amplitudes of the four arrivals in Figure 3, we obtained the coda-free amplitudes of these arrivals (Figure 6): $A_P \approx 1.7$, $A_{P410P} \approx 4.1$, $A_{WG} \approx 2.1$, $A_{WGfs} \approx 2.9$, $\lambda \approx 0.22$. During this joint inversion of the energy envoelopes, we also found that a value of Q=380 better describes the observed pattern of overlapping codas than the value of Q=320 estimated from the cumulative linear trend in Figure 4.

Figure 6 shows that the simple model (3) describes the observed amplitude pattern satisfactorily throughout the entire recording time range. As expected, the strongest phase in the deconvolved amplitude pattern in the bottom of Figure 6 is the reflection from the 410-km discontinuity. Note that because of increased attenuation below about 150-km depth (Morozov *et al*., 1998a, b), the arrivals from the mantle transition zone are very weak in the high-pass filtered records and they do not boost the apparent WG energy (Figure 3).

3. Mantle waveguide focusing under the profiles QUARTZ and RUBY?

As the argument above shows, the energies of secondary phases including the long-range P_n appear stronger than they are in reality due to their enhancement by the codas of the earlier phases. However, even after our amplitude correction, the amplitudes of the WG modes, and in particular, their total energy (Figure 6, bottom) are still significantly higher than expected from 1-D modeling (Mechie *et al*., 1993; Morozova *et al*., 1999). At longer ranges, high amplitudes of the surface multiples of P_n in this region are also indicated by the observations of a very strong *PP* phase (corresponding to the first phase in the WG_{fs} group in our notation) from the Semipalatinsk nuclear explosions (Baumgardt, 1985, 1990).

As a solution to this controversy, we suggest that high amplitudes of the waves guided within the lithosphere could be their focusing under the northern part of the East European Platform. This region has a mantle structure that is distinctly different from that of the West Siberian basin (Mechie et al., 1997; Morozova et al., 1999). The unusually high amplitudes of the long-range P_n have been observed only on the profiles QUARTZ and RUBIN traversing the East European platform (Ryberg et al., 1995), and the strong *PP* phase was also identified along a the path close to that of the profile RUBIN (Figure 1; Baumgardt, 1985). On the contrary, our preliminary study suggests that the long-range P_n is much weaker and crustal attenuation is somewhat lower under the Siberian craton .

Although still qualitative, the above argument is supported by an observation that not only the *WG* arrivals but also their primary phases P_n, and P_N (the latter are refractions and reflections from regional seismic boundaries between 90 – 140 km depth; cf. Pavlenkova, 1996; Morozova *et al*., 1999) are very strong between the offsets of about 300 – 800 km (Figure 2). Such strong amplitudes should be due to high energy of the source and to the velocity gradient and reflectivity observed within the lithosphere (Morozova *et al*., 1999). After a reflection from the Moho and free surface, this near-critical energy could form the observed strong waveguide arrivals (WG in Figure 3).

The high amplitudes of multiple refractions (*PP* and *WG*) could be explained by the effects of crustal, Moho, and lithospheric heterogeneity favoring propagation of energy within the top 150 – 200 km of the mantle under the northern part of the East European platform and under the West Siberian basin (Figure 1). Among these effects are the strong velocity gradient and reflecting boundaries in the uppermost mantle (Morozova *et al*., 1999). As demonstrated by Kennett (1987), within the ranges of PNE profiles (20° to 30°) layered structures within the mantle may act as a wave-guide contributing significantly to the *P*-wave coda.

Baumgardt (1985) also suggested that focusing could explain the high-amplitude *PP* in NORSAR recordings of the Semipalatinsk nuclear explosions. In particular, near-receiver focusing was required to account for the variations of *PP* amplitude across the array. In contrast to this observation, QUARTZ records show consistent and strong WG phases within the entire offset range and suggest that reflective lithosphere with vertical velocity gradient and favorable source conditions should be responsible for the overall character of the wavefield. Near-receiver scattering manifests itself in reduced coherency between the adjacent seismograms.

The unusually strong P_n and WG phases observed in QUARTZ records could support the observations of coda flattening between 310 – 450 sec after the teleseismic *P*-wave arrival in the recordings of Semipalatinsk explosions at NORSAR (Baumgardt, 1985, 1990). In a detailed study, Baumgardt (1990) showed that this part of the coda consisted primarily of L_g and S_n modes, with minor amounts of P_n energy and no detectable teleseismic *P* contribution. He interpreted this coda flattening as a result of $P_n \rightarrow L_g$ scattering under the Urals. This explanation, which appears to be the only reasonable model of the observed coda, also implies that the P_n is strong and carries enough energy to reverse the decay of the *P*-wave coda.

4. The nature of the PNE arrival coda

Since our coda decay model in equation (2) is dictated simply by the scattering geometry and by the principle of conservation of energy, it should be applicable to other observations of scattering at regional and teleseismic distances. Indeed, in a teleseismic study of underground nuclear explosions at Novaya Zemlya, Greenfield (1971) interpreted the observed coda as a result of near-source $R_g \rightarrow P$ scattering and pointed out that without crustal attenuation, the coda energy would have been constant. Dainty (1990) suggested that for Kazakh nuclear tests recorded at NORESS, about half of the coda energy consisted of near-source $L_g \rightarrow P$ scattering, and another half was represented by $P \rightarrow L_g$ scattering near the seismic array, with an energy decay law similar to derived above (Dainty, 1985). Baumgardt (1985, 1990) used incoherent beams and continuous "polar scans" to identify variations in coda decay and mode content within 200 – 400 sec of the teleseismic *P*-wave codas.

The codas of the WG phases and, as we suggested above, of all the other *P*-wave phases are not due to anomalously low crustal attenuation and to a tuned, narrow-band, highly scattering uppermost mantle as suggested by Ryberg *et al*. (1995) or by Ryberg and Wenzel (1999). On the contrary, we favor the traditional interpretation of the coda as a result of crustal scattering of the waves incident from the mantle and propagating at high apparent velocities. The reciprocity principle complements this mechanism by its counterpart in which strong crustal-guided waves (P_g, S_g, L_g, R_g) generated by the PNE are scattered on crustal heterogeneities producing secondary phases propagating through the mantle and feeding the observed coda (Dainty, 1985, 1990).

The observed difference between the amplitude dependencies of the records at lower and higher frequencies (Figure 3) is very significant. Similarly to the deep *P*-wave phases, the WG_{fs} arrival and its coda are low in their high-frequency content. Compared to *WG*, WG_{fs} is similar but travels two additional passes through the crust, and thus the disappearance of WG_{fs} in the high-pass filtered record should be related to crustal attenuation. Also, the increased *Q* at higher frequencies (Figure 4) and its regional variations (Figure 3) suggests that the low-frequency coda contains more surface waves sampling the sedimentary, lower-*Q* parts of the upper crust. Therefore, the difference between *WG* and WG_{fs} also points to a crustal nature of the coda.

An important implication of our coda model is that only a three-dimensional (3-D) analysis of scattering can yield reasonable quantitative estimates of the dynamic properties of the PNE wavefield. Although 3-D or 2-D modeling of PNE short-period records using realistic crustal and mantle models is at present not practical, it appears that interpretations of scattering based exclusively on 1-D simulations (Tittgemeyer, 1996; Ryberg and Wenzel, 1999) might become misleading. On the contrary, energy balance considerations consistent with the accepted teleseismic coda models and utilizing the true, 3-D view of the process of wave propagation allow us to explain the behavior of the coda and to unravel the amplitude relations between the observed PNE phases.

5. Using receiver functions to map crustal basement

In another application of the new, amplitude and waveform analysis of PNE records, we computed receiver function sections by deconvolving the vertical-component record of each PNE seismogram from profile QUARTZ from the corresponding inline component. The receiver function sections from the three QUARTZ PNEs were stacked and correlated with the detailed crustal model derived earlier (Morozova et al., 1999; Figure 7); in this model, the depths to the basement were obtained from industry reflection and borehole data and was provided by the Center GEON, Moscow.

A comparison (Figure 7, middle) of the detailed picks of the crustal basement with the receiver function image shows that although the Moho P/S conversion cannot be correlated in the receiver function stack, the basement is well pronounced as a *P* to *S* converted arriving 1 – 2 sec after the first arrivals. Although such conversions generally contribute to the complexity of the first-arrival waveforms and cannot be picked directly, deconvolution reveals the variations of the depth of the basement with substantial detail. Among possible implications of this observation, we suggest that (1) receiver functions computed using the 3-component recordings of PNE first arrivals can be used to constrain such important structural features of the crust as the depth to the basement, and (2) it shows that P/S conversions on the basement and other resonances within the sediments contribute to the complexity and amplitudes of the first (and presumably all other) arrivals. Both of these conclusions should be considered carefully during modeling of Lg propagation in realistic crustal structures like the one presented in Figure 7, top.

CONCLUSIONS AND RECOMMENDATIONS

Based an analysis of amplitude envelopes of the records from the profile QUARTZ, we arrived at both a consistent explanation of the character of PNE arrival coda as well as at a realistic estimate of its decay rate, in contrast to some of the previous results (Ryberg *et al*., 1995; Tittgemeyer *et al*., 1996; Ryberg and Wenzel, 1999). The key points of our coda model of PNE arrivals are:

1) A long coda detectable to 100 – 150 sec in DSS records follows every PNE arrival at an offset range over 2000 km;

2) Codas of the long-range arrivals are due to scattering within the crust of the primary PNE arrivals propagating at high apparent velocities thus leading to distributed coda excitation and reduced geometric spreading;

3) The codas of the PNE arrivals build up energy within the record section leading to an increased energy within the *PP* time window. This amplitude pattern of the records was inverted for true amplitude relations between the arrivals.

As a result of our PNE coda model, we obtained estimates of coda *Q* ranging between Q_0=380 near 2 Hz and Q_0=430 around 5 Hz. These values correspond to the values generally associated with the crust (including the sedimentary rocks) and suggest that the crust could be the source of the extensive coda pattern observed in PNE

records (Figure 3). As our study shows, the amplitude pattern of the PNE records throughout their full length can be explained quantitatively by body- and guided waves within the upper mantle and by (predominantly) crustal scattering.

Using receiver function analysis of PNE arrivals, we show that scattering and P/S conversions within the crust cause reverberations in the waveforms of *P*-wave arrivals. Stacked receiver functions of first arrivals produced a consistent images of the basement along the PNE profile QUARTZ. This technique could potentially be used for imaging crustal basement along other PNE and conventional-explosion profiles with 3-component recordings.

REFERENCES

Aki, K. and B. Chouet (1975). Origin of coda waves: source, attenuation, and scattering effects, *J. Geophys. Res.,* 80*,* 3,322-3,342.

Bannister, S. G., E. S. Husebye, and B. O. Ruud (1990). Teleseismic *P* coda analyzed by three-component and array techniques: deterministic location of topographic *P*-to-*Rg* scattering near the NORESS array, *BSSA*, 80, 1969-1986.

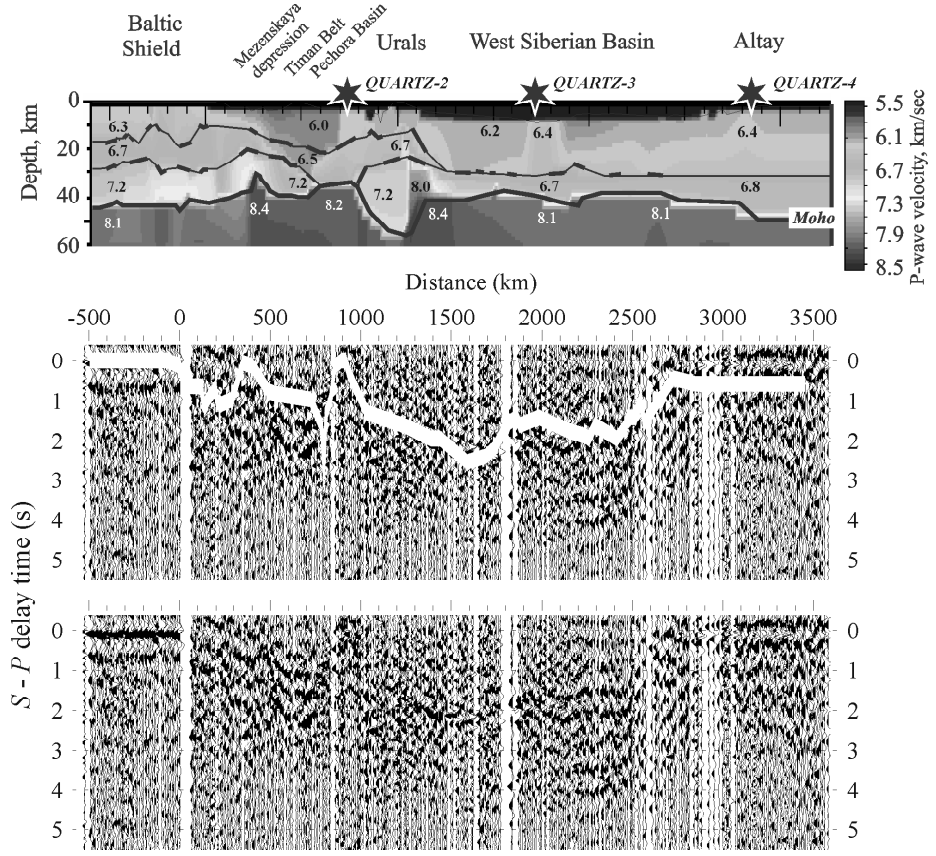

Figure 7 Mapping the crustal basement using receiver functions. *Top*: detailed crustal and uppermost mantle velocity model from profile QUARTZ (same as in Fig. 2). *Middle* and *bottom*: interpreted and uniterpreted stacked receiver function sections from the three QUARTZ PNEs. The white line in the middle plot is the zoomed in profile of the basement from our crustal model scaled to *S – P* wave delay time. Note the good fit of the basement depth with the stacked receiver function. Also note that such a detailed basement profile cannot be obtained from a travel-time interpretation of QUARTZ data (it was derived from industry reflection, higher-resolution DSS, and borehole data, and provided by GEON), but, remarkably, it wss obtained here from the PNE data alone.

Baumgardt, D. R. (1985). Comparative analysis of teleseismic *P* coda and *Lg* waves from underground nuclear explosions in Russia, *Bull. Seism. Soc., Am*., 75, 1413-1433.

Baumgardt, D. R. (1990). Investigation of teleseismic *Lg* blockage and scattering using regional arrays, *Bull. Seism. Soc., Am*., 80, 2261-2281.

Campillo, M. (1987). *Lg* wave propagation in a laterally varying crust and the distribution of the apparent quality factor in central France, *J. Geophys. Res.,* 92, 12604-12614.

Dainty, A. M. (1985). Air Force Geophysical Laboratory Report, AFGL-TF-86-0218.

Dainty, A. M. (1990). Studies of coda using array and three-component processing, *PAGEOPH*, 132, 221-244.

Greenfield, R. J. (1971). Short-period *P*-wave generation by Rayleigh-wave scattering at Novaya Zemlya, *JGR*, 76, 7988-8002.

Gupta, I.N., T. W. McElfresh, and R. A. Wagner (1991). Near-source scattering of Rayleigh to *P* in teleseismic arrivals from Pahute Mesa (NTS shots, in: Taylor, S. R., H. J. Patton, and P. G. Richards (Eds.), Explosion Source Phenomenology, *AGU Geophys. Monograph*, 65, 151 - 160.

Kennett, B. L. N. (1987). Observational and theoretical constraints on crustal and upper mantle heterogeneity, *Phys. Earth Planet. Interiors*, 47, 319-332.

Mechie, J., A. V. Egorkin, K. Fuchs, T. Ryberg, L. Solodilov, and F. Wenzel (1993). P-wave velocity structure beneath northern Eurasia from long-range recordings along the profile Quartz, *Phys. Earth Planet Inter*., 79, 269-286.

Mechie, J., A. V. Egorkin, L. Solodilov, K. Fuchs, F. Lorenz, and F. Wenzel (1997). Major features of the mantle velocity structure beneath northern Eurasia from long-range seismic recordings of peaceful nuclear explosions, *in:* Fuchs, K. (Ed.) Upper mantle heterogeneities from active and passive seismology, pp. 33-50, Kluwer Academic Publ., Dordrecht.

Morozov, I. B. Comment on "High-frequency wave propagation in the uppermost mantle" by T. Ryberg and F. Wenzel, *J. Geophys. Res*., in press.

Morozov, I., B., E. A. Morozova, and S. B. Smithson, (1997). Observation of *Lg* and *S* wave propagation along the ultra-long profile "Quartz", Russia, *in:* Fuchs, K. (Ed.) Upper mantle heterogeneities from active and passive seismology, Kluwer, pp. 147-154.

Morozov, I., B., E. A. Morozova, and S. B. Smithson, (1998a). On the nature of the teleseismic *Pn* phase observed in the recordings from the ultra-long profile "Quartz", Russia, *Bull. Seism. Soc. Am.*, 88, 62-73.

Morozov, I., B., E. A. Morozova, and S. B. Smithson, (1999). Preliminary characterization of l_g phase propagation from Peaceful Nuclear Explosions in Siberia, Russia, 21 DoD/DoE Seismic Research Symposium, Las Vegas, NV, September, 1999.

Morozov, I., B., E. A. Morozova, S. B. Smithson, and L. N. Solodilov (1998b). 2-D image of seismic attenuation beneath the Deep Seismic Sounding profile QUARTZ, Russia, *Pure Appl. Geoph*, 153, 311-343.

Morozova, E. A., I. B. Morozov, S. B. Smithson, and L. N. Solodilov (1999). Heterogeneity of the uppermost mantle beneath the ultra-long range profile "Quartz," Russian Eurasia, *J. Geophys. Res*., 104 (B9), 20,329-20,348.

Ryberg, T., and F. Wenzel (1999). High-frequency wave propagation in the uppermost mantle, *J. Geophys. Res.,* 104*,* 10,655-10,666.

Ryberg, T., K. Fuchs, A. V. Egorkin, and L. Solodilov (1995). Observations of high-frequency teleseismic P_n on the long-range Quartz profile across northern Eurasia, *J. Geophys. Res.,* 100*,* 18151-18163.

Singh, S., and R. B. Herrmann (1983). Regionalization of crustal coda *Q* in the Continental United States, *J. Geophys. Res*., 88, 527-538.

Sultanov, D. D., J. R. Murphy, and Kh. D. Rubinstein, 1999. A seismic source summary for Soviet Peaceful Nuclear Explosions, *Bull. Seism. Soc. Am.,* 89, 640-647.

Tittgemeyer, M., F. Wenzel, K. Fuchs, and T. Ryberg (1996). Wave propagation in a multiple-scattering upper mantle—observations and modeling, *Geophys. J. Int.,* 127, 492-502.